Three-dimensional resolvability in an integral imaging system

Zahra Kavehvash,[1,*] Manuel Martinez-Corral,[2] Khashayar Mehrany,[1] Saeed Bagheri,[3] Genaro Saavedra,[2] and Hector Navarro[2]

[1]*Department of Electrical Engineering, Sharif University of Technology, P.O. Box 11365-8639, Tehran, Iran*
[2]*Department of Optics, University of Valencia, E-46100 Burjassot, Spain*
[3]*Philips Research North America, 345 Scarborough Road, Briarcliff Manor, New York 10510, USA*
**Corresponding author: kavehvash@ee.sharif.edu*

Received November 22, 2011; revised January 23, 2012; accepted January 23, 2012; posted January 27, 2012 (Doc. ID 158712); published March 21, 2012

The concept of three-dimensional (3D) resolvability of an integral imaging system is thoroughly investigated in this research. The general concept of 3D resolution fails to describe the 3D discrimination completely. Then the concepts of the depth-resolution plane and lateral-resolution plane are introduced to show the difference between the conventional 3D spatial resolution and the newly introduced 3D resolvability. Therefore, the different properties of these planes for differentiating lateral spatial variations and axial variations are analyzed in this paper. The theoretical statements are demonstrated experimentally.

OCIS codes: 110.6880, 110.3000.

1. INTRODUCTION

Three-dimensional (3D) imaging systems have attracted interest in different scientific and commercial fields, such as 3D TV, computer games, engineering design, and virtual reality, to name a few. There are several types of 3D imaging technologies (i.e., capturing, processing, and displaying), which are broadly divided into two categories, stereoscopic and autostereoscopic. While in past years most of the research in the area of 3D imaging systems has concentrated on stereoscopic technology [1–3], the fact that the viewer had to wear special eyeglasses in order to see the 3D effect has limited the acceptance and the application of them. The autostereoscopic display systems are more comfortable for the viewer as they do not require the use of special glasses and provide the viewer with full parallax [4]. Holography [5–6], volumetric displays [7], and integral imaging are types of autostereoscopic technology. Holographic technology offers parallax in all directions but the need for coherent light sources and dark room conditions during recording, reduces its practical utility. Volumetric display systems often have large field of view. However, their application has been limited because of the difficulty to design them. Integral imaging (InI), based on the integral photography concept proposed in 1908 by Lippmann [8], recently reattracted researcher interest, due to its desired properties such as capturing many views in real time. InI offers many advantages as opposed to other existing 3D sensing techniques, as it uses natural light, can offer full parallax in real time, and does not require special glasses [9]. Therefore, it constitutes a promising technology for the production of real-time 3D image capture and display systems. In the past few years, as microlens manufacturing has been progressing, offering further flexibilities to InI, much effort has been devoted in order to overcome some significant problems of InI. Such shortcomings are the limited depth of field (DOF) [10–12] and the low quality of the displayed images [13].

The main reason for the low quality of InI is the limited resolution of the reconstructed image. This limited resolution is due to the limited number of pixels in each elemental image (EI) and the large pitch period of the lens array. Many researchers have focused their work on improving the resolution of the output 3D images by either improving the number of pixels in each EI or decreasing the lens pitch [14–21]. Therefore, in all of these works the resolution improvement was done in the EI side while the real effect on the 3D image side was not investigated thoroughly. This is due to the fact that the concept of resolution in a 3D InI system is complicated. The most comprehensive work in this area is by Hoshino *et al.* [22], Burckhardt [23], and Okoshi [24]. Hoshino *et al.* [22] studied the effects of the EI resolution and the lens pitch on the quality of the formed 3D image. They made some conclusions about how the appropriate values of the EI bandwidth and the lens pitch depend on the viewer distance. Burckhardt [23] and later Okoshi [24] examined the 3D resolvability by combining the concepts of lateral and depth resolutions. All these works suffer from two major points of weakness. First, they are not applicable when the 3D image is to be constructed computationally. This is due to the fact that they are all based on the visualization concept and thus depend on the viewer's position and field of view. Second, they do not consider the effects of the display device pixel size and the number of lenses in the array. These points are addressed in this paper, where the concept of 3D resolvability is based on the concepts of sampling rays and sampling points. The usefulness of the proposed concept is confirmed through experiments. This manuscript is organized as follows: Section 2 explains the concept of the proposed definition of 3D resolvability in InI systems describing the concept of sampling rays, sampling points, and the numerical algorithms for extraction of sampling points in different subsections. Section 3 confirms the claimed concepts by presenting some experiments. Finally, in Section 4 the main achievements of this paper are summarized.

2. 3D RESOLVABILITY IN INTEGRAL IMAGING SYSTEMS

In this section we first introduce the concept of sampling rays. This concept is already defined in 2D imaging systems, but it is here applied to establish the concept of 3D sampling points. Distinctive features of 3D sampling points making them useful in investigation of the concept of 3D resolution are then examined in 3D InI systems. To better illustrate the applicability of the introduced concept, two particular kinds of planes, namely, the "lateral-resolution plane" and "depth-resolution plane," are introduced to demonstrate two extreme scenarios of 3D resolvability in InI systems.

A. Sampling Rays

For simplicity's sake, the concept of sampling ray is introduced in a single lens imaging system. It is here assumed that the sensor of the imaging system is at distance g from the lens and has a small yet nonzero pixel size. If obtaining the maximum DOF is aimed, it is convenient to focus the lens at the hyperfocal distance [25]. This distance depends on the pixel size, the f-number, and also on the focal length of the lenslets. In this case, all objects at distances from half of the hyperfocal distance out to infinity will be acceptably sharp. Given that the principal ray [26] connecting the center of each pixel to the center of the lens transfers the object information to the pixel, the principal ray can be referred to as the sampling ray. It should be noted that the lens has a limited resolution and thus the object information is in fact carried by a sampling beam rather than a sampling ray. Nevertheless, each sampling beam can be reasonably approximated by a sampling ray because the object information is captured if the object is within the DOF range, where the sampling beam has a negligible width (equal to the lens spot size).

It is true that once the sampling beam is approximated by the sampling ray, the unwanted effects incurred by the limited resolution of the single lens are neglected. Notwithstanding, the concept of sampling rays is proved to be useful when there is more than one lens in the imaging system. This is shown in the next subsection, where the concept of the 3D sampling point is introduced.

B. Sampling Points and 3D Resolvability

The reconstruction stage in a typical 3D InI system is schematically shown in Fig. 1. Although in the figure we still depict the lenslets, in fact, the reconstruction algorithms work by projecting the center of the pixels through virtual pinholes placed at the center of the lenslets. Thus, the algorithms are totally independent on the lenslets' focal length. The sampling rays emanating from each pixel of each EI passing through the center of its corresponding lens are depicted by solid lines. It should be noted that the sampling rays passing through each of the lenses must remain within its field of view (FOV). In accordance with the previous subsection, the sampling rays convey the object information from each EI to the DOF region and thus contribute to the 3D image reconstruction. Given that the image can be reconstructed at an arbitrary vertical plane $z = z_i$ lying within the DOF region, any such plane is hereafter referred to as the image plane. The cross section of a sampling ray and an image plane is then called a zeroth-order sampling point. Thanks to the information conveyed by the sampling rays, the higher is the number of the zeroth-order sampling points at the image planes, the better the lateral resolution becomes.

In a 3D InI system based on a lens array, however, different types of sampling points exist because different sampling rays emanating from different lenslets in the array can cross each other and form a specific sampling point. For instance, the cross points of two different sampling rays coming from two different lenslets are referred to as the first-order sampling points. They are marked by circles at the specific image plane $z = z_i$ in Fig. 1. Similarly, the cross section of $(n + 1)$ sampling rays forms the nth-order sampling points. It is worth noting that there are an infinite number of zeroth-order sampling points because there are an infinite number of image planes lying between z_L and z_R but there are only a finite number of first-order sampling points.

The distinctive feature of the nth-order sampling points $(n \geq 1)$ is that they have a good depth resolution. This is due to the fact that the nth-order sampling point is reconstructed by using $(n + 1)$ sampling rays coming from $(n + 1)$ different EIs. The nth-order sampling point is thus easily differentiated from its neighboring zeroth-order sampling points lying on each one of the $(n + 1)$ sampling rays. It is worth noting that the information contributed by each one of the $(n + 1)$ sampling rays comes from different direction. On the one hand, it is desirable to reconstruct the image at the plane where as many sampling rays as possible are crossing with each other, i.e., where we have the highest order sampling

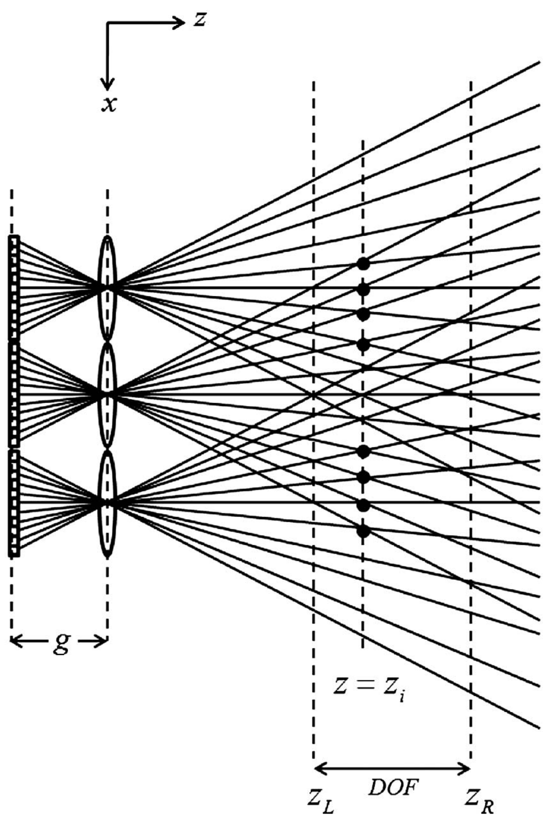

Fig. 1. Principal ray pattern in InI together with the first-order sampling points marked by circles.

points. This plane is hereafter referred to as the depth-resolution plane because it has the best depth resolution. On the other hand, it is desirable to reconstruct the image at the plane where we have the largest number of sampling points and thus the highest lateral resolution. Because increasing the order of sampling points at each specific image plane decreases the total number of sampling points at the same plane, the lateral resolution is bought at the expense of the depth resolution. The image plane with the maximum number of first-order sampling points, whose depth resolution is not as bad as that of the zeroth-order sampling points, is hereafter referred to as the lateral-resolution plane. The lateral and depth resolutions of different image planes lying within the DOF region are both in this fashion studied by using the here-proposed concepts of the sampling points. Given that the 3D resolution is a mixture of the lateral and depth resolutions, studying the distribution of the sampling points reveals the 3D resolvability at different image planes.

C. Numerical Algorithm for Extraction of Sampling Points

To extract the coordinates of the sampling points in the 3D InI system, the line equation of sampling rays is needed. Because the sampling ray emanated from the i, jth pixel of the p, qth EI coincides with the principal ray passing through its corresponding lenslet in the array, the line equation of the sampling rays can be written in terms of the i, jth pixel coordinates (x_i, y_j, $-g$) and the p, qth lenslet (x_p, y_q, 0):

$$\frac{z+g}{g} = \frac{x - x_i}{x_p - x_i} = \frac{y - y_j}{y_q - y_j}, \tag{1}$$

where g is the distance between the EIs shown on the display device and the lens array. It should be pointed out that the sampling ray must lie within the FOV of the lens and thus the following two equations ought to be held:

$$\tan^{-1}\left(\frac{x_p - x_i}{g}\right) \le \alpha_x \tan^{-1}\left(\frac{y_q - y_j}{g}\right) \le \alpha_y, \tag{2}$$

where α_x and α_y are the lens FOV in x and y directions. The coordinates of the zeroth-order sampling points at the image plane z_i are obtained straightforwardly:

$$(x_0, y_0, z_0) = \left(\frac{(z_i + g)(x_p - x_i)}{g} + x_i, \frac{(z_i + g)(y_q - y_j)}{g} + y_j, z_i\right). \tag{3}$$

The coordinates of the higher order sampling points are not as easy to obtain. The coordinates of the first-order sampling points are extracted by finding the intersection of two different sampling rays emanating from different EIs. To this end, the following set of equations is to be solved:

$$\begin{cases} \frac{x - x_i}{x_p - x_i} = \frac{x - x_{i'}}{x_{p'} - x_{i'}} \\ \frac{y - y_j}{y_q - y_j} = \frac{y - y_{j'}}{y_{q'} - y_{j'}} \\ \frac{x_p - x_i}{g}(z + g) + x_i = \frac{x_{p'} - x_{i'}}{g}(z + g) + x_{i'} \end{cases}, \tag{4}$$

where $p, q \ne p', q'$, ensuring that the sampling rays are coming from different EIs (sampling rays coming from the same EI do not cross with each other). The obtained coordinates are acceptable if its z coordinate is lying between z_L and z_R.

Similarly, the coordinates of the nth-order sampling points are extracted by finding the intersection of $(n+1)$ sampling rays. This time, however, the number of equations is more than the number of unknown coordinates, as we have a set of $3n$ equations with three unknown coordinates. It should be noted, however, that we have an nth-order sampling point not only when $(n+1)$ sampling rays are passing through the same point, but also when they are in a close proximity to each other. For this reason, the coordinates of the nth-order sampling point are extracted by finding the specific coordinates whose overall error in satisfaction of all of the $3n$ equations lie below a threshold level. Once again, the thus obtained coordinate is acceptable if its z coordinate is lying between z_L and z_R.

D. Influential Parameters

It is the aim of this subsection to show how different parameters of the 3D InI system affect the distribution of the sampling points and thereby control the 3D resolvability. Increasing the total number of pixels on the display device increases the overall number of sampling rays and augments the chance of having higher order sampling points. It is therefore beneficial for both the lateral and depth resolutions. Decreasing the lens pitch, on the other hand, decreases the sampling rays and thus deteriorates the lateral resolution but increases the number of higher order sampling points. It is thus advantageous for the depth resolution. Increasing the FOV of each lens increases the overall number of sampling rays and thus the total number of higher order sampling points. It is therefore expected to be advantageous for both the lateral and depth resolutions. It should be noted, however, that increasing the FOV deteriorates the lens resolution by increasing the spot size. This latter effect is neglected in extraction of the sampling points because sampling beams in our approach are replaced by sampling rays. Consequently, increasing the FOV is more effective on increasing the depth resolution. Finally, increasing the number of EIs or lenslets in the array increases the number of sampling rays and thus the zeroth-order sampling points. It is for this reason good for the lateral resolution. It should be pointed out, however, that increasing the number of EIs or lenslets beyond a certain level does not increase the number of higher order sampling points because the sampling

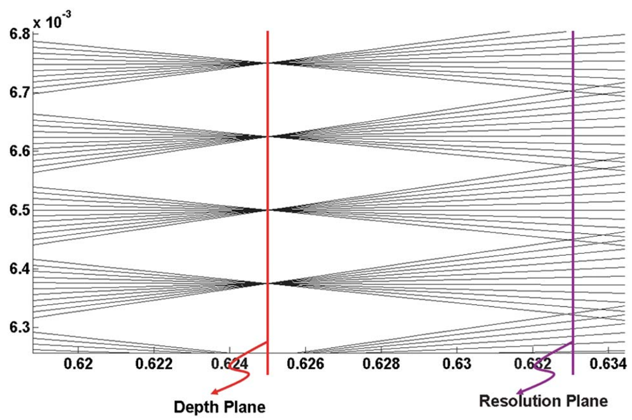

Fig. 2. (Color online) Enlarged part of ray patterns with the specified location of the depth- and lateral-resolution planes.

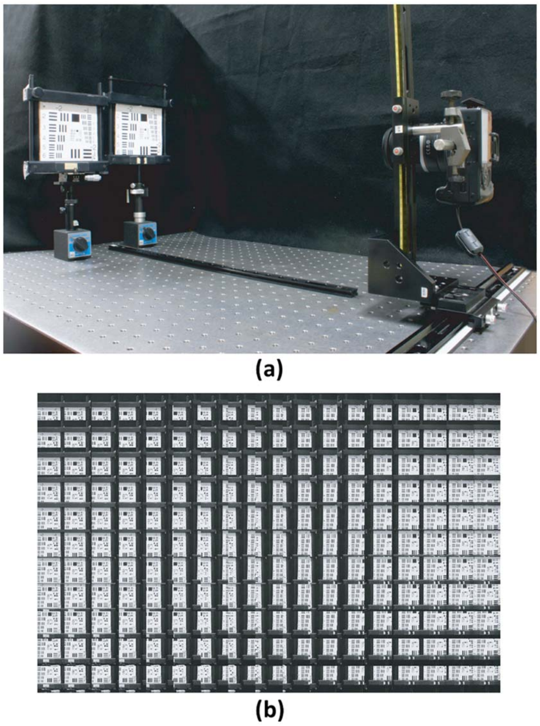

Fig. 3. (Color online) (a) Experimental setup used in the first experiment and (b) the resulting EI array.

rays will be too far from each other to cross each other within the DOF region.

3. EXPERIMENTS

In this section, to better demonstrate the proposed concepts we have performed some experiments. The first experiment is done using the standard resolution charts. The reason for choosing these charts is for more accurate demonstration of the properties of different lateral planes in preserving different frequency contents. In this scenario we have selected a depth-resolution plane and a lateral-resolution plane that are very close to each other. The reason for this selection is to better demonstrate the depth discrimination property of the depth planes. Here we have performed the experiment with 11×17 EIs with 200×200 pixels per EI and a lens pitch of 10 mm. The distance between the EI array plane and the lens array is $g = 50$ mm while we are imaging in the focused mode. In the first step we drove the patterns of all rays emanating from the EIs' pixels and passing through the lenses in the array. The depth- and lateral-resolution planes are found by following the numerical algorithm as described in Subsection 2.3. Using the system of coordinates shown in Fig. 1, the depth and lateral resolution planes are at $z =$ 62.5 and 63.3 cm, respectively. The sampling rays passing through the x–z plane are shown in Fig. 2, where the depth

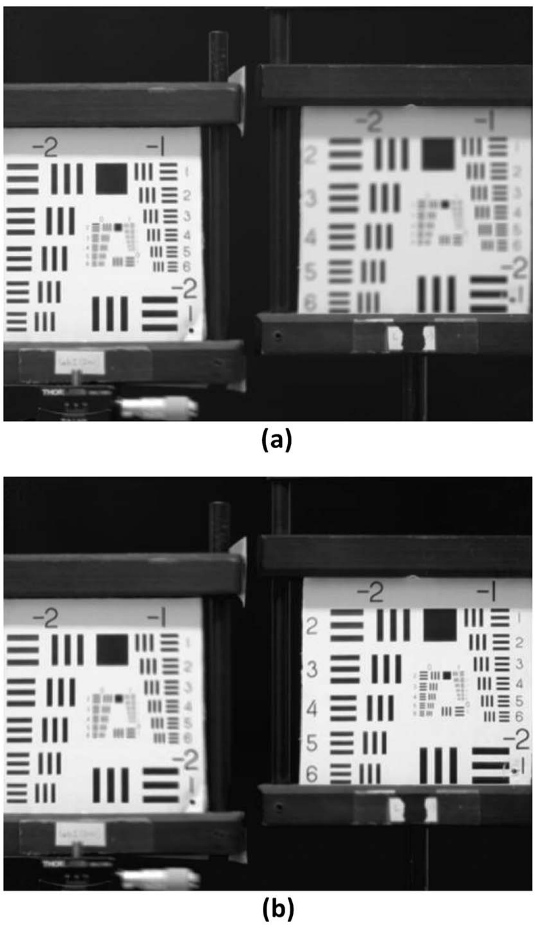

Fig. 4. Reconstructed image of the resolution charts in the (a) depth plane and (b) resolution plane.

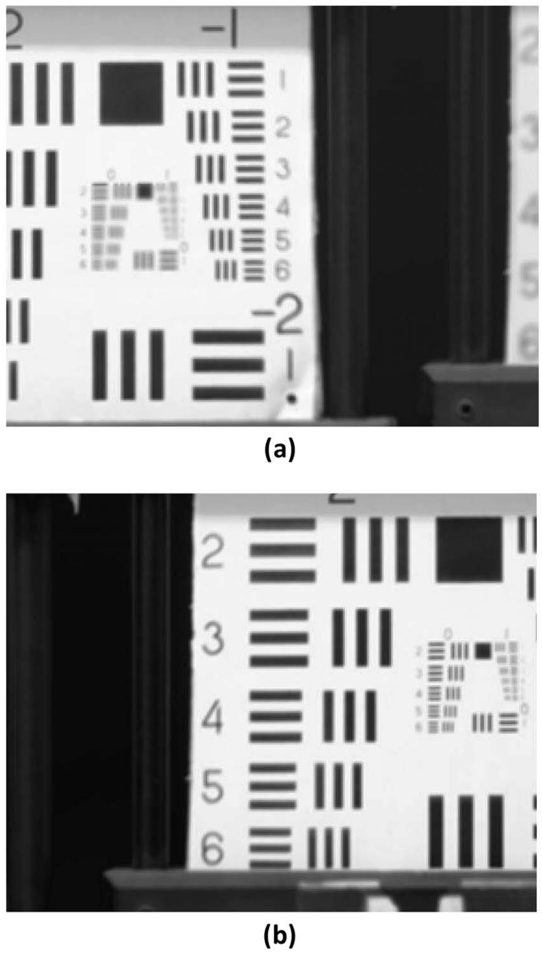

Fig. 5. Enlarged high-frequency parts of the reconstructed image of resolution charts in the (a) depth plane and (b) resolution plane.

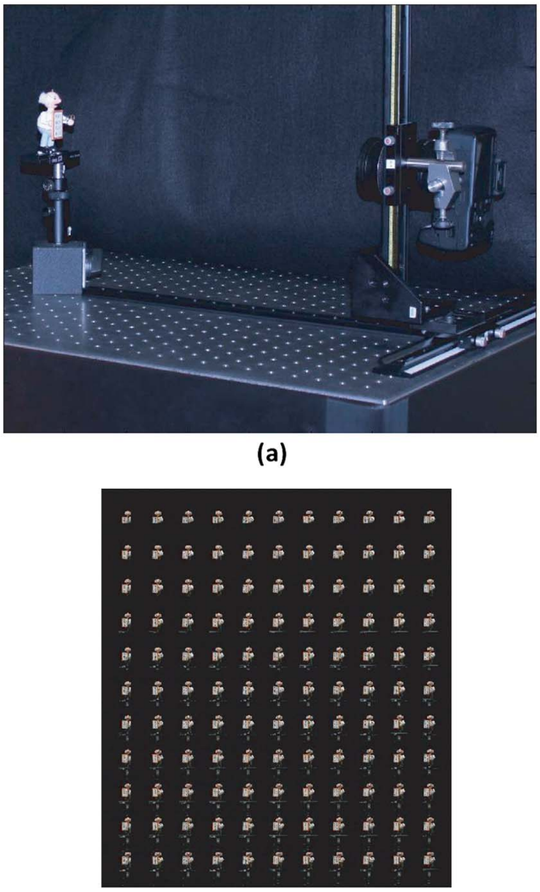

(a)

(b)

Fig. 6. (Color online) (a) Setup used in the second experiment and (b) resulting EI array.

and lateral resolution planes are also marked. It can be easily seen that the depth-resolution plane has fewer sampling points of a higher order while the lateral-resolution plane has more sampling points of a lower order. It should be pointed out that there are many planes having a large number of first-order sampling points; therefore, finding the plane with the absolute maximum number of first-order sampling points is not necessary. Rather, the plane with the local maximum number of the first-order sampling points lying in proximity of the depth-resolution plane is here found to better demonstrate the idea of the depth resolvability. Then we have placed a resolution chart in the depth-resolution plane and another one in the lateral-resolution plane. The setups used for the recording stage and the recorded EI array are shown in Figs. 3(a) and 3(b), respectively. Then we performed reconstruction computationally in both selected depth and lateral resolution planes [27]. The reconstructed images are shown in Figs. 4(a) and 4(b), respectively. The resolution chart in the left part is in the depth-resolution plane, and the right-side chart is placed in the lateral-resolution plane. It is clearly noticeable from the reconstructed images that depth discrimination is done better in the depth-resolution plane. In reconstructing in the depth-resolution plane (the plane of the left chart), the out-of-focus object is more blurred compared to the image resulted from reconstruction in lateral-resolution plane. To compare the resolution in two planes, we have shown in Fig. 5 an enlarged section of the two images including the high-frequency contents. It is apparent from the figures that the high-frequency contents are better preserved in the lateral-resolution plane, while when using the depth-resolution plane as the imaging plane, the axial resolution is better conserved.

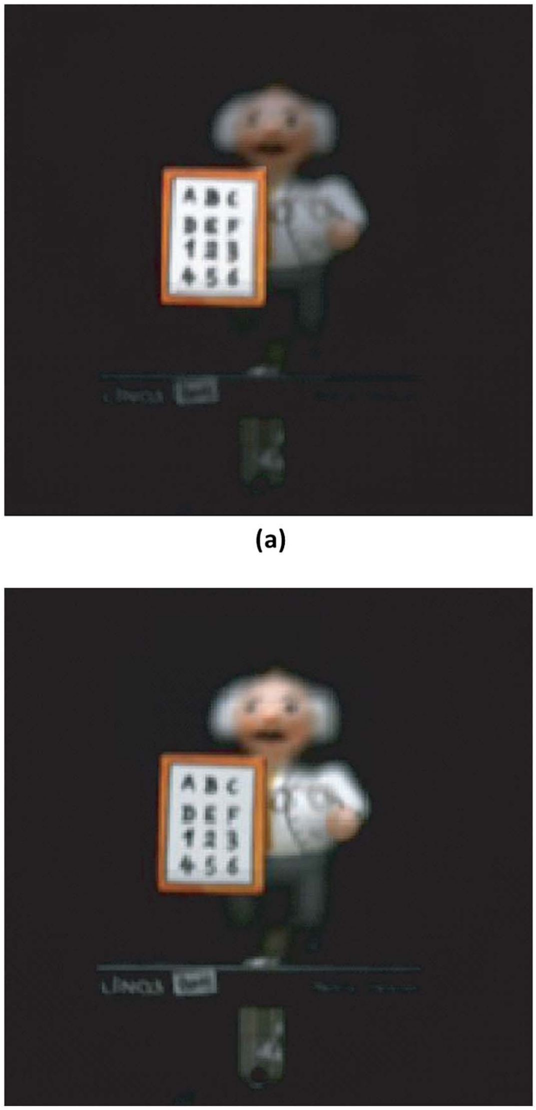

(a)

(b)

Fig. 7. (Color online) Reconstructed images of optometrist while the board is in the (a) depth plane and (b) resolution plane.

In the second experiment, we have selected a more real object to show the analyzed 3D resolvability property of InI systems. The selected object is an optometrist with a resolution board in his hand. In this experiment, we have used an array of 11×11 lenses with gap $g = 35$ mm, while each EI is composed of 201×201 pixels. Similarly, the depth- and lateral-resolution planes are found. The lateral-resolution plane is at $z = 35.0$ cm, and the depth-resolution plane is at 35.2 cm. Then we recorded two sets of EIs. For the first set, we placed the optometrist so that the board was set at the depth-resolution plane. In the second, the board was set at the lateral-resolution plane. The experimental setup and the recorded EIs for depth-resolution plane imaging are shown in Figs. 6(a) and 6(b), respectively.

Again we performed computational reconstruction for the two imaging planes using the two sets of captured EIs. The resulting images in the depth- and lateral-resolution planes are shown in Figs. 7(a) and 7(b), respectively. Again, the expected properties are clearly noticeable. In the depth-resolution-plane image, the board is more distinctly reconstructed than the other out-of-focus parts of the image, while in the lateral-resolution plane, the other parts of the image that are not in the reconstruction plane are also as distinguishable as the written board. On the other hand, the resolution of the board is better preserved in lateral-resolution-plane imaging as the letters on the board are reconstructed more visibly.

4. CONCLUSION

We proposed a new definition for 3D resolvability in an InI system. Despite previous definitions that were just based on visualization, here the concept is explained more thoroughly using ray optics. The concept of lateral and axial resolvability was explained based on geometrical optics and sampling properties of rays and ray crossing. Then two different imaging planes were introduced; one of them had appropriate depth resolution, and the other one resolved lateral points more accurately. The selection between these imaging planes depends on the amount of desired 3D resolution in the lateral and axial (depth) directions. To better demonstrate the analyzed properties, two experiments were presented: one with standard resolution charts and the other with a real object. The result of the experiments verifies the claimed concepts and features. In our future works, we are going to also consider the effect of eye and observer's distance along the ray crossing on the 3D resolution. The other related work will be designing the InI system for the purpose of better axial or lateral resolution.

ACKNOWLEDGMENTS

Zahra Kavehvash acknowledges the financial support of the Iran Research Institute for Information and Communication Technology. Manuel Martinez-Corral, Genaro Saavedra, and Hector Navarro also acknowledge support from the Ministerio de Ciencia e Innovación, Spain (grant FIS2009-9135), and from the Generalitat Valenciana (grant PROMETEO2009-077).

REFERENCES

1. T. Okoshi, *Three-Dimensional Imaging Techniques* (Academic, 1976).
2. S. M. Faris, "Novel 3D stereoscopic imaging technology," Proc. SPIE **2177**, 180–195 (1994).
3. S. Yano, S. Ide, T. Mitsuhashi, and H. Thwaites, "A study of visual fatigue and visual comfort for 3D HDTV/HDTV images," Displays **23**, 191–201 (2002).
4. N. A. Dodgson, "Autostereo displays: 3D without glasses," presented at EID '97: Electronic Information Displays, Esher, Surrey, November 18–20 1997.
5. C. Slinger, C. Cameron, and M. Stanley, "Computer-generated holography as a generic display technology," Computer **38**, 46–53 (2005).
6. R. B. A. Tanjung, X. Xu, X. Liang, S. Solanki, Y. Pan, F. Farbiz, B. Xu, and T.-C. Chong, "Digital holographic three-dimensional display of 50-Mpixel holograms using a two-axis scanning mirror device," J. Opt. Eng. **49**, 025801 (2010).
7. B. G. Blundell, A. J. Schwarz, and D. K. Horrell, "Volumetric three-dimensional display systems: their past, present and future," Eng. Sci. Educ. J. **2**, 196–200 (1993).
8. M. G. Lippmann, "La photographie intégrale," C.R. Acad. Sci. **146**, 446–551 (1908).
9. W. Ijsselsteijn, H. de Ridder, and J. Vliegen, "Effects of stereoscopic filming parameters and display duration on the subjective assessment of eye strain," Proc. SPIE **3957**, 12–22 (2000).
10. M. Martinez-Corral, B. Javidi, R. Martinez-Cuenca, and G. Saavedra, "Integral imaging with improved depth of field by use of amplitude modulated microlens array," Appl. Opt. **43**, 5806–5813 (2004).
11. R. Martinez-Cuenca, G. Saavedra, M. Martinez-Corral, and B. Javidi, "Enhanced depth of field integral imaging with sensor resolution constraints," Opt. Express **12**, 5237–5242 (2004).
12. A. Castro, Y. Frauel, and B. Javidi, "Integral imaging with large depth of field using an asymmetric phase mask," Opt. Express **15**, 10266–10273 (2007).
13. J.-S. Jang and B. Javidi, "Improved viewing resolution of three-dimensional integral imaging by use of nonstationary micro-optics," Opt. Lett. **27**, 324–326 (2002).
14. A. Stern and B. Javidi, "Three-dimensional image sensing and reconstruction with time-division multiplexed computational integral imaging," Appl. Opt. **42**, 7036–7042 (2003).
15. Z. Kavehvash, Kh. Mehrany, and S. Bagheri, "Spatial frequency multiple access technique in three-dimensional integral imaging," J. Display Technol., **8**, 138–144 (2012).
16. Z. Kavehvash, Kh. Mehrany, and S. Bagheri, "Field of view extension using frequency division multiple access technique: numerical analysis," Proc. SPIE **8043**, 80430F (2011).
17. Y. Kim, J. Kim, J. M. Kang, J. H. Jung, H. Choi, and B. Lee, "Point light source integral imaging with improved resolution and viewing angle by the use of electrically movable pinhole array," Opt. Express **15**, 18253–18267 (2007).
18. J. S. Jang, Y. S. Oh, and B. Javidi, "Spatiotemporally multiplexed integral imaging projector large-scale high-resolution three-dimensional display," Opt. Express **12**, 557–563 (2004).
19. H. Liao, M. Iwahara, N. Hata, and T. Dohi, "High-quality videography using a multiprojector," Opt. Express **12**, 1067–1076 (2004).
20. H. Liao, T. Dohi, and M. Iwahara, "Improved viewing resolution of integral videography by use of rotated prism sheets," Opt. Express **15**, 4814–4822 (2007).
21. M. Martinez-Corral and G. Saavedra, "The resolution challenge in 3D optical microscopy," *Progress in Optics*, Vol. 53, E. Wolf, ed. (Elsevier, 2009), pp. 1–67.
22. H. Hoshino, F. Okano, H. Isono, and I. Yuyama, "Analysis of resolution limitation of integral photography," J. Opt. Soc. Am. A **15**, 2059–2065 (1998).
23. C. B. Burckhardt, "Optimum parameters and resolution limitation of integral photography," J. Opt. Soc. Am. A **58**, 71–76 (1968).
24. T. Okoshi, "Optimum design and depth resolution of lens-sheet and projection-type three-dimensional displays," Appl. Opt. **10**, 2284–2291 (1971).
25. R. Kingslake, *Lenses in Photography: The Practical Guide to Optics for Photographers* (Garden City, 1951).
26. M. Born and E. Wolf, *Principles of Optics: Electromagnetic Theory of Propagation, Interference and Diffraction of Light* (Cambridge University, 1997).
27. S. H. Hong, J. S. Jang, and B. Javidi, "Three-dimensional volumetric object reconstruction using computational integral imaging," Opt. Express **12**, 483–491 (2004).